The ozonolysis of ethylene. Microwave spectrum, molecular structure, and dipole moment of ethylene primary ozonide (1,2,3-trioxolane)

ARTICLE *in* JOURNAL OF THE AMERICAN CHEMICAL SOCIETY · APRIL 1988

Impact Factor: 12.11 · DOI: 10.1021/ja00232a007

4 AUTHORS, INCLUDING:

R.D. Suenram
University of Virginia
247 PUBLICATIONS **6,654** CITATIONS
SEE PROFILE

Francis J. Lovas
National Institute of Standards and Techn…
286 PUBLICATIONS **8,940** CITATIONS
SEE PROFILE

The Ozonolysis of Ethylene. Microwave Spectrum, Molecular Structure, and Dipole Moment of Ethylene Primary Ozonide (1,2,3-Trioxolane)

J. Z. Gillies,*,† C. W. Gillies,† R. D. Suenram,‡ and F. J. Lovas‡

Contribution from the Department of Chemistry, Rensselaer Polytechnic Institute, Troy, New York 12180-3590, and Molecular Spectroscopy Division, National Bureau of Standards, Gaithersburg, Maryland 20899. *Received May 4, 1988*

Abstract: The gas-phase structure of ethylene primary ozonide ($\overline{CH_2CH_2OOO}$) has been determined from millimeter wave spectra of five isotopic species. Partial substitution, r_s, parameters for the lowest energy oxygen envelope conformation (C_s symmetry) are r(CC) = 1.546 (3) Å, r(CO) = 1.417 (10) Å, r(OO) = 1.453 (10) Å, $r(CH_{endo})$ = 1.088 (5) Å, $r(CH_{exo})$ = 1.095 (5) Å, θ(CCO) = 103.9 (2)°, θ(COO) = 102.1 (4)°, θ(OOO) = 100.1 (12)°, and θ(HCH) = 111.6 (3)°. The electric dipole moment of the normal isotopic species is 3.43 (4) D. Two vibrational states, 98 (6) and 171 (18) cm^{-1} above the ground state, have been assigned to successive excitations of the pseudorotational mode which corresponds to a ring-twisting vibration of the five-membered ring. The barrier to pseudorotation is estimated to be high (greater than 300 to 400 cm^{-1}) in agreement with ab initio MO calculations. Ethylene primary ozonide, dioxirane ($\overline{CH_2OO}$), formaldehyde, and ethylene secondary ozonide ($\overline{CH_2OCH_2OO}$) are observed as products of the ozone–ethylene reaction in the low-temperature microwave cell. A mechanism of the ozonolysis of ethylene is presented which suggests that the reaction occurs primarily in the condensed phase on the surface of the cell. Microwave techniques utilizing *cis*- and *trans*-CHD=CHD show that ozone adds stereospecifically to ethylene in the formation of ethylene primary ozonide.

The ozonolysis of alkenes is used for synthetic purposes in organic chemistry to produce carbonyl compounds by oxidative cleavage of carbon–carbon double bonds.[1] Gas-phase reactions of ozone with alkenes are of particular importance to air pollution in the troposphere.[2] The reaction mechanism has been extensively studied in solution[1,3] and the gas phase.[4,5] A three-step sequence outlined below was proposed by Criegee in the 1950s.[6] If ste-

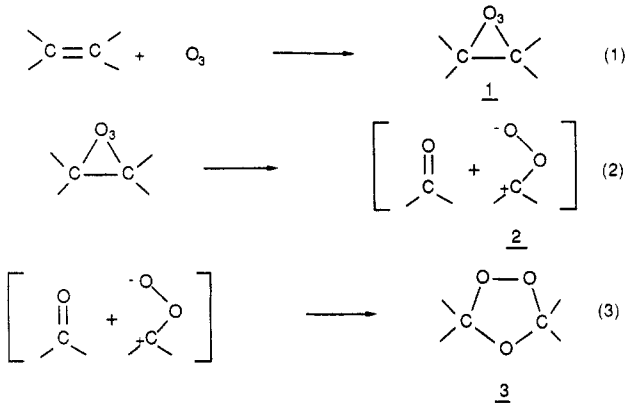

reochemical effects are ignored, the mechanism rationalizes secondary ozonide (SO) **3** formation through the Criegee intermediate, dioxymethylene **2**, which is produced in step 2.

The initial adduct, **1**, is called the primary ozonide (PO). Although Criegee did not specify its structure at the time, the first step is now thought to be a concerted 1,3-dipolar cycloaddition between ozone and an alkene.[1,3] Hence, **1** is expected to have the 1,2,3-trioxolane structure.

In solution ozonolyses of a number of alkenes, there is chemical and spectroscopic evidence which shows that thermally unstable intermediates are formed at low temperature. These chemical species precipitate out of solution[7] and some can be converted to diols.[7a,d,f] NMR studies of a few *cis*- and *trans*-dialkyl-substituted alkenes confirm the existence of the PO and also show that the cis POs are considerably less stable than the trans POs.[8] A combination of the chemical and NMR studies provides strong evidence that the addition of ozone to these *cis*- and *trans*-dialkyl-substituted alkenes is stereospecific.

Solution and solid matrix infrared spectra are known for a number of POs.[9] Disappearance of some PO spectra is correlated with the appearance of the SO in step 3. In cases where POs are observed by both NMR and IR, the decomposition temperatures agree quite well.

There is no one prior experimental study which unequivocally determines the molecular structure of POs in the condensed phases. However, the 1,2,3-trioxolane structure is very reasonable for the PO when all the chemical and spectroscopic data are considered together. No evidence has been published which proves the existence of a PO in the gas phase. Consequently, the molecular structures of free POs have been investigated solely by a variety of semiempirical and ab initio quantum chemical calculations.[10]

† Rensselaer Polytechnic Institute.
‡ National Bureau of Standards.

(1) Bailey, P. S. *Ozonation in Organic Chemistry*; *Academic Press*: New York, 1978, Vol. 1; 1982, Vol. 2.
(2) Niki, H.; Maker, P. D.; Savage, C. M.; Breitenbach, L. P. *Environ. Sci. Technol.* **1983**, *17*, 312A.
(3) Kuczkowski, R. L. *1,3-Dipolar Cycloadditions*; Padwa, A., Ed.; Wiley: New York, 1984; p 197.
(4) Herron, J. T.; Martinez, R. I.; Huie, R. E. *Int. J. Chem. Kinet.* **1982**, *14*, 201.
(5) Kafafi, S. A.; Martinez, R. I.; Herron, J. T. *Molecular Structure and Energetics*; Liebman, J. F., Greenburg, A., Eds.; VCH Publishers: Deerfield Beach, FL, 1988; Chapter 10.
(6) Criegee, R. *Rec. Chem. Prog.* **1957**, *18*, 111.
(7) (a) Criegee, R.; Schröder, G. *Chem. Ber.* **1960**, *93*, 689. (b) Criegee, R. *Peroxide Reaction Mechanisms*; Edwards, J. O., Ed.; Wiley-Interscience: New York, 1962; p 29. (c) Greenwood, F. L.; Cohen, S. *J. Org. Chem.* **1963**, *28*, 1159. (d) Greenwood, F. L. *J. Org. Chem.* **1964**, 29, 1321. (e) Greenwood, F. L.; Haske, B. J. *Tetrahedron Lett.* **1965**, 631. (f) Greenwood, F. L. *J. Org. Chem.* **1965**, 30, 3108. (g) Ramachandran, V.; Murray, R. W. *J. Am. Chem. Soc.* **1978**, *100*, 2197. (h) Fong, G. D. *Diss. Abst. B* **1979**, *39*, 4907.
(8) (a) Bailey, P. S.; Thompson, J. A.; Shoulders, B. A. *J. Am. Chem. Soc.* **1966**, *88*, 4098. (b) Durham, L. J.; Greenwood, F. L. *J. Chem. Soc., Chem. Commun.* **1967**, 843. (c) Durham, L. J.; Greenwood, F. L. *J. Org. Chem.* **1968**, *33*, 1629. (d) Durham, L. J.; Greenwood, F. L. *J. Chem. Soc., Chem. Commun.* **1968**, 24. (e) Bailey, P. S.; Ferrell, T. M., Rustaiyan, A.; Seyhan, S.; Unruh, L. E. *J. Am. Chem. Soc.* **1978**, *100*, 894.
(9) (a) Hull, L. A.; Hisatsune, I. C.; Heicklen, J. *J. Am. Chem. Soc.* **1972**, *94*, 4856. (b) Alcock, W. G.; Mile, B. *J. Chem. Soc., Chem. Commun.* **1976**, 5. (c) Nelander, B.; Lord, L. *Tetrahedron Lett.* **1977**, *32*, 2821. (d) Hisatsune, I. C.; Kolopajlo, L. H.; Heicklen, J. *J. Am. Chem. Soc.* **1977**, *99*, 3704. (e) Hisatsune, I. C.; Shinoda, K.; Heicklen, J. *J. Chem. Soc.* **1979**, *101*, 2524. (f) Nelander, B.; Lord, L. *J. Am. Chem. Soc.* **1979**, *101*, 3769. (g) Mile, B.; Morris, G. W.; Alcock, W. G. *J. Chem. Soc., Perkin Trans.* **1979**, *2*, 1644. (h) Kohlmiller, C. K.; Andrews, L. *J. Am. Chem. Soc.* **1981**, *103*, 2578.

0002-7863/88/1510-7991$01.50/0

In our recently reported microwave study,[11] ethylene PO (CH_2CH_2OOO) was detected in the gas phase by condensing ozone and ethylene on the walls of a microwave absorption cell and allowing the reaction to occur by warming up the cell. This method was used previously in the discovery of dioxirane employing similar reaction conditions.[12] The ethylene PO work demonstrated that **1** has the 1,2,3-trioxolane structure.[11] The lowest energy conformation was shown to be an oxygen envelope with C_s symmetry.

This paper provides a full report of the first spectroscopic detection of ethylene PO in the gas phase. Deuterium, carbon-13, and oxygen-18 isotopic substitutions are used to obtain a complete gas-phase structure of ethylene PO from rotational constant data. Bond moments are derived from the electric dipole moment data, and two low-lying vibrational states are assigned to successive excitations of a ring puckering mode. A mechanism for the ozonolysis of ethylene in the low-temperature microwave absorption cell is proposed which describes the formation of ethylene PO, dioxirane, formaldehyde, and ethylene SO. The stereospecificity of the addition of ozone to ethylene is studied directly by microwave techniques utilizing *cis*- and *trans*-1,2-dideuterioethylene.

Experimental Section

Spectroscopy. An 80-kHz Stark-modulated spectrometer was used for all the microwave measurements obtained in this work. The absorption cell which was a 1-m stainless steel waveguide in K_u band (12–18 GHz) and the gas-handling system have been described previously.[12] The millimeter wave sources were phase locked reflex klystrons operated under computer control.[13] The detectors consisted of commercially available, low-noise, point-contact Schottky barrier diodes. Peak absorption frequencies were obtained by adding up–down computer scans of the observed transitions and fitting the data to Gaussian line shapes. The absorption lines were broad with full-widths at half-peak intensities of typically 2 MHz. All the frequency measurements listed in Table I have an uncertainty of 0.2 MHz.

Dipole moment measurements of the normal isotopic species of ethylene PO were obtained with the 80-kHz spectrometer by coupling a dc voltage to the 80-kHz square wave. The $J = 3 \leftarrow 2$, $M_J = 2 \leftarrow 2$ Stark transition of OCS was used to determine the average Stark electrode spacing.[14]

Ethylene Ozonolyses. Ethylene PO was synthesized directly in the K_u band absorption cell using the methods described previously for the dioxirane study.[12] First, ozone is expanded into the cell from a silica gel trap maintained at dry ice temperature. Then the cell is cooled to liquid nitrogen temperature and uncondensed gas is pumped away. Ethylene is slowly introduced into the waveguide. After the ethylene has condensed on the walls of the cell, residual gas is pumped out, and the temperature is allowed to gradually increase. *Caution: Mixing ozone and ethylene together under these conditions presents an explosion hazard.* It is estimated that less than 0.1 mmol of ozone and ethylene were used for a given experiment. When a larger amount of ozone was used on one occasion, an explosion resulted which ripped a 10-cm hole in the thin wall stainless steel absorption cell. It is recommended that this reaction not be carried out in a glass apparatus.

When the cell warms to −175 °C, there is a pressure surge and the temperature rises rapidly to −170 °C. At temperatures above −170 °C the pressure is maintained at 30–75 μm by continuously pumping on the cell. The temperature of the cell is controlled by flowing precooled nitrogen gas through the stainless steel jacket which surrounds the absorption cell.

Rotational spectra from products and intermediates produced in the reaction at very low temperature appear at higher temperatures where the vapor pressures of these species are sufficient to observe transitions. At −130 °C formaldehyde is observed, followed by dioxirane and ethylene SO in the range of −115 to −100 °C. Transitions arising from ethylene PO are first seen at ~−115 °C and attain maximum intensity at −100 °C. It is possible to observe the ethylene PO spectrum at −100 °C for up to 5 or 6 h from a single reaction while continuously pumping on the sample. Under these conditions, the dioxirane spectrum becomes very weak. When the temperature is increased to −90 °C, the ethylene PO transitions disappear while the ethylene SO lines continue to gain spectral intensity and the dioxirane spectrum reappears. For the rotational assignment of ethylene PO, the temperature was kept at −100 to −95 °C.

Isotopic modifications of ethylene PO were synthesized by the methods described above for the normal isotopic species; 90% enriched [1,2-^{13}C]ethylene was used to prepare $^{13}CH_2{}^{13}CH_2OOO$. *trans*-$CHDCHDOOO$ was synthesized from 99% deuterium-enriched *trans*-CHD=CHD, while the two cis isomers of $CHDCHDOOO$ were prepared from 99% enriched *cis*-CHD=CHD. CD_2CD_2OOO was synthesized from 99% enriched CD_2=CD_2. Using methods described previously, oxygen-18 enriched ozone was made from 99% enriched $^{18}O_2$.[12] Trisubstituted ^{18}O ethylene PO was made from the $^{18}O_3$ and CH_2=CH_2.

Results

Millimeter Wave Spectra. A molecular identification and spectral assignment of ethylene PO were reported previously.[11] The rotational spectrum consisted of *b*-type, high *J*, Q-branch series and *b*-type R-branch transitions. Since the molecule is a nearly oblate rotor with $\kappa = +0.66$ [$\kappa = (2B - A - C)/(A - C)$], the series origin of the *b*-type Q-branch lines is approximated by the expression:

$$\nu = (A + B - 2C)(K_{+1} + \tfrac{1}{2}) \quad \text{(I)}$$

Equation I which is derived in the Appendix was used to identify the Q-branch series of all the isotopic species of ethylene PO. *A*, *B*, and *C* are the rotational constants in MHz and K_{+1} is the oblate top quantum number.

The spectral assignments for the enriched isotopic species were obtained in the way described for the normal isotopic species.[11] Once Q-branch lines were assigned, it was possible to identify strong lines which consisted of degenerate pairs of high *J*, low K_{-1}, R-branch transitions. Additional nondegenerate R-branch lines were necessary to complete the centrifugal distortion analysis. Table I lists the observed *b*-type transitions of all enriched isotopic species. The frequency data were fit to the rotational constants and to four quartic centrifugal distortion constants using the Watson Hamiltonian and the *A* reduction calculation.[15] Table II gives the spectral constants obtained from the least-squares fit of the lines listed in Table I.

Since fewer transitions were observed for CD_2CD_2OOO, the frequency data could be fit to the three rotational constants and only three quartic centrifugal distortion constants. The fourth distortion constant, δ_J, was held constant at the value determined for the normal isotopic species.[11] Table III lists the observed transition frequencies and the spectral constants for CD_2CD_2OOO.

Dipole Moment. The electric dipole moment of ethylene PO was determined from measurements of frequency shifts and applied electric fields for the $M_J = 0$, 1, 2, and 3 Stark components of the $5_{5,0}$–$4_{4,1}$ line and the $M_J = 1$ and 2 Stark components of the $9_{4,5}$–$8_{5,4}$ line. A total of 49 values of frequency shifts, $\Delta\nu$, versus electric field squared, E^2, were least-squares fit to second-order Stark theory[16] according to the equation:

$$\Delta\nu = E^2\mu_a{}^2[A(a) + B(a)M_J{}^2] + E^2\mu_b{}^2[A(b) + B(b)M_J{}^2] + E^2\mu_c{}^2[A(c) + B(c)M_J{}^2] \quad \text{(II)}$$

The constants $A(a)$, $B(a)$, $A(b)$, $B(b)$, $A(c)$, and $B(c)$ are the second-order Stark coefficients for the transition. μ_a, μ_b, and μ_c are the electric dipole components along the three principal axes. All the *A* and *B* Stark coefficients were calculated from the energy

(10) (a) Renard, J.; Fliszár, S. *J. Am. Chem. Soc.* **1970**, *92*, 2628. (b) Rouse, R. A. *J. Am. Chem. Soc.* **1973**, *95*, 3460. (c) Hiberty, P. *J. Am. Chem. Soc.* **1976**, *98*, 6088. (d) Klopman, G.; Andreozzi, P. *Bull. Soc. Chim. Belg.* **1977**, 86, 481. (e) Cremer, D. *J. Chem. Phys.* **1979**, *70*, 1898. (f) Cremer, D. *J. Chem. Phys.* **1979**, 70, 1911. (g) Cremer, D. *J. Chem. Phys.* **1979**, *70*, 1928. (h) Ruoff, P.; Almlof, J.; Saebo, S. *Chem. Phys. Lett.* **1980**, *72*, 489. (i) Ruoff, P.; Saebo, S.; Almlof, J. *Chem. Phys. Lett.* **1981**, *83*, 549.

(11) Zozom, J.; Gillies, C. W.; Suenram, R. D.; Lovas, F. J. *Chem. Phys. Lett.* **1987**, *140*, 64.

(12) Suenram, R. D.; Lovas, F. J. *J. Am. Chem. Soc.* **1978**, *101*, 5117.

(13) Suenram, R. D.; Lovas, F. J. *J. Am. Chem. Soc.* **1980**, *102*, 7180.

(14) Reinartz, J. M. L. J.; Dymanus, A. *Chem. Phys. Lett.* **1974**, *24*, 346.

(15) Watson, J. K. G. *J. Chem. Phys.* **1967**, *46*, 1935.

(16) Golden, S.; Wilson, E. B. *J. Chem. Phys.* **1948**, *16*, 669.

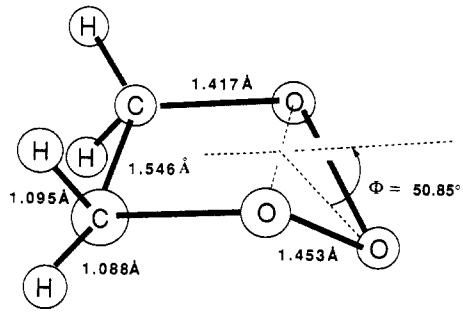

Figure 1. The observed lowest energy gas-phase conformation of ethylene PO oxygen envelope with C_s symmetry.

levels utilizing the rotational constant data in Table II. The analysis determined $\mu_a = 0.00$ (1) D, $\mu_b = 3.39$ (4) D, and $\mu_c = 0.500$ (5) D which gives a total electric dipole moment of 3.43 (4) D.

Molecular Structure. Comparison of the observed rotational constants of the normal isotopic species with those calculated for a variety of possible molecular structures of **1** indicated that the observed spectrum arose from a 1,2,3-trioxolane structure. The electric dipole moment measurements confirmed this result by proving that the species has C_s symmetry with nonzero *b* and *c* dipole components.[11] Out of all possible conformations for the 1,2,3-trioxolane ring, only an oxygen envelope form with C_s symmetry is consistent with the spectral constants and electric dipole data.[11]

The isotopic work provides further independent evidence that ethylene PO has the oxygen envelope conformation with C_s symmetry. Only the oxygen envelope conformation has nonequivalent pairs of hydrogen substituents in which the two pairs are oriented exo or endo with respect to the apex ring oxygen (Figure 1). This conformation produces two cis forms of 1,2-dideuterioethylene PO. The two deuterium atoms must be located in either the endo or exo positions in order to have a cis configuration. The rotational spectra of these two cis isotopic species are different since the hydrogen atom coordinates are not equivalent. In contrast, only one *trans*-1,2-dideuterioethylene PO is possible for the oxygen envelope conformation because the trans configuration requires one deuterium in an endo site and the second deuterium in an exo position.

Two cis forms of 1,2-dideuterioethylene PO were observed and their rotational spectra assigned (Tables I and II) from the reaction of ozone with *cis*-CHD=CHD. Despite extensive spectral searching, the rotational spectrum of only one trans form of 1,2-dideuterioethylene PO was assigned (Tables I and II) as expected for the oxygen envelope conformation having C_s symmetry. In this case, the trans isomer of 1,2-dideuterioethylene PO was produced from the reaction of ozone with *trans*-CHD=CHD.

The oxygen envelope form of ethylene PO has 14 atomic coordinates which are required to completely determine the molecular structure. Moments of inertia data reported previously for the normal isotopic species[11] may be combined with the isotopic data listed in Table II to calculate the structure in several different ways. Chutjian's double substitution equations[17] give the exo and endo hydrogen coordinates, the $oxygen_{1,3}$ *a* coordinate, and the carbon *a* and *b* coordinates. The remaining small carbon *c* coordinate and the four oxygen *b* and *c* coordinates are determined by a least-squares fit[18] to the six *b* and *c* second moments of the normal isotope, the oxygen-18 isotope and the *trans*-dideuterio isotope as well as the two nontrivial center of mass relations ($\sum_i m_i b_i = 0$, $\sum_i m_i c_i = 0$) and the nontrivial cross product equation ($\sum_i m_i b_i c_i = 0$).

Table IV lists the atomic coordinates obtained from the method described above. The p-r_s structure (partial substitution) derived from these coordinates is given in Table V. In order to get an estimate of structural uncertainties due to zero-point vibrational effects, the 14 atomic coordinates were least-squares fit[18] to the first moment, cross product, and second moment equations for all isotopic species except $\overline{CD_2CD_2OOO}$, for which the spectral constants were not as well determined (see Table III). This r_0 method provides 21 equations for the determination of 14 coordinates. Tables IV and V list the r_0 atomic coordinates and structural parameters obtained from this fit.

The propagated errors in the p-r_s structural parameters were determined from Costain uncertainties in the p-r_s atomic coordinates. These uncertainties are given in parentheses next to the p-r_s parameters in Table V. Costain uncertainties provide unrealistically large estimates of small coordinate uncertainties such as the carbon *c* coordinates. The standard deviation from the least-squares fit which determined the small carbon *c* coordinate provides a better estimate of this coordinate uncertainty.[19] The propagated errors in the p-r_s structural parameters which depend upon the carbon *c* coordinate were obtained using the least-squares estimate of the uncertainty in the carbon *c* coordinate. The standard deviations in the atomic coordinates from the complete r_0 least-squares fit were used to get the propagated error in the r_0 structure. These estimates of the uncertainties are given in parentheses adjacent to the r_0 parameters in Table V.

Comparison of the p-r_s and r_0 parameters reveals differences of over 0.01 Å in bond lengths and of more than 1° for some bond angles. These differences arise largely from the $oxygen_{1,3}$ and $oxygen_2$ *b* coordinates which vary over 0.01 Å depending upon the choice of moment equations used in the least-squares fitting. Generally, the r_s substitution structure is preferred since vibrational effects tend to cancel by this method.[20] However, the need to fit the small carbon *c* coordinate and the four *b* and *c* coordinates for oxygen leads to only one true r_s parameter, the carbon–carbon bond distance, in the molecule. It is somewhat arbitrary to prefer the p-r_s or r_0 structure for the other parameters. Hence, the uncertainties in these bond distances and angles should be taken as the larger of two numbers: either the difference between the p-r_s and r_0 structures or the estimated uncertainties listed in Table V. The Costain uncertainty is a conservative estimate of the uncertainty in the preferred r_s C–C bond distance.

Discussion

Molecular Conformation. The microwave data establish that ethylene PO has the 1,2,3-trioxolane structure with C_s symmetry. As shown in Figure 1, this lowest energy form corresponds to an oxygen envelope conformation in which the unique oxygen is bent out of the plane defined by the remaining four ring atoms. Details of the spectral evidence from the normal isotopic species were published previously and are not repeated here.[11] The isotopic data obtained in the present work confirm the earlier conclusions and also provide a full gas-phase structure.

Semiempirical and ab initio techniques have been used extensively to determine the molecular structure and lowest energy conformations of primary ozonides.[10] The motivation for these calculations was due in part to interest in the mechanism of ozonolysis where certain conformations of the primary ozonide were assumed to rationalize the stereochemistry of secondary ozonide formation.[1,3] However, the theoretical work has yielded a variety of conflicting results.

Extended-Hückel theory finds that the carbon–carbon half-chair form is of lower energy than the oxygen envelope conformer shown in Figure 1.[10a,21] Rouse demonstrated that CNDO/2 calculations place the carbon–oxygen half-chair and carbon envelope conformers lowest in energy.[10b] The complete geometry optimized structure at the MINDO/3 level corresponds to a slightly distorted planar structure.[10d] The earliest ab initio studies did not include

(17) Chutjian, A. *J. Mol. Spectrosc.* **1964**, *14*, 361.
(18) The structural fitting program STRFIT was developed by Dr. R. H. Schwendeman, Department of Chemistry, Michigan State University, East Lansing, MI 48824.
(19) Harmony, M. D.; Laurie, V. W.; Kuczkowski, R. L.; Schwendeman, R. H.; Ramsay, D. A.; Lovas, F. J.; Lafferty, W. J.; Maki, A. G. *J. Phys. Chem. Ref. Data* **1979**, *8*, 619.
(20) Costain, C. C. *J. Chem. Phys.* **1958**, *29*, 864.
(21) See ref 10e and 11 for descriptions of the various nonplanar conformations of the 1,2,3-trioxolane ring.

Table I. Rotational Transitions (MHz) of Carbon-13, Oxygen-18, and Deuterium Isotopomers of Ethylene Primary Ozonide

transition	$^{13}CH_2{}^{13}CH_2OOO$		$CH_2CH_2{}^{18}O{}^{18}O{}^{18}O$		*trans*-CHDCHDOOO		*cis,endo*-CHDCHDOOO		*cis,exo*-CHDCHDOOO	
$J'_{K_{-1},K_{+1}} - J''_{K_{-1},K_{+1}}$	ν_{obsd}[a]	$\Delta\nu$[b]	ν_{obsd}[a]	$\Delta\nu$[b]	ν_{obsd}[a]	$\Delta\nu$[b]	ν_{obsd}[a]	$\Delta\nu$[b]	ν_{obsd}[a]	$\Delta\nu$[b]
$6_{5,2}-5_{2,3}$			107 124.27	−0.01						
$7_{6,1}-6_{5,2}$			106 359.57	−0.06	106 479.44	0.27				
$7_{7,1}-6_{6,0}$	109 398.65	−0.05	107 112.94	−0.04	103 465.49	−0.39			102 605.85	−0.11
$7_{7,0}-6_{6,1}$	110 291.90	0.12	107 428.78	0.01	104 463.10	−0.02			104 317.70	0.49
$8_{6,3}-7_{5,2}$			108 429.34	−0.04					102 590.89	0.22
$8_{7,2}-7_{6,1}$			117 836.73	0.02	113 132.95	−0.02				
$8_{8,1}-7_{7,0}$					118 695.83	−0.16			117 799.34	−0.25
$8_{8,0}-7_{7,1}$					119 286.28	−0.01				
$9_{1,8}-8_{2,7}$							84 646.56	−0.11		
$9_{5,5}-8_{4,4}$							103 361.90	−0.13	102 745.13	0.12
$9_{6,4}-8_{5,3}$			113 791.93	0.06	110 202.12	0.19	110 831.59	0.06		
$9_{4,5}-8_{5,4}$							103 196.50	0.33	102 720.85	0.15
$9_{5,4}-8_{6,3}$			106 744.90	0.01	108 664.33	−0.08	108 579.00	−0.13	108 928.68	−0.34
$9_{6,3}-8_{7,2}$					110 631.62	−0.07				
$10_{4,7}-9_{3,6}$	109 424.42	0.07							104 558.20	0.00
$10_{5,6}-9_{4,5}$			111 797.01	0.46[c]	111 246.06	0.29	111 620.93	0.02	110 942.60	−0.72
$10_{3,7}-9_{4,6}$							105 393.38	0.28		
$10_{6,5}-9_{5,4}$					117 724.29	0.09	118 136.77	−0.07	117 393.00	0.14
$10_{4,6}-9_{5,5}$			111 640.58	−0.04	111 236.05	0.10	111 601.43	0.01		
$10_{5,5}-9_{6,4}$			117 460.08	−0.56[c]	117 477.26	0.26	117 714.33	0.05	117 329.70	−0.09
$11_{2,10}-10_{1,9}$	104 469.85	−0.06								
$11_{3,9}-10_{2,8}$	111 229.11	0.11								
$11_{2,9}-10_{3,8}$			106 902.40	0.00			107 575.70	−0.34[c]		
$11_{5,7}-10_{4,6}$							119 965.54	−0.72[c]		
$11_{3,8}-10_{4,7}$			113 388.28	0.40[c]	113 252.21	0.09	113 762.65	0.10	112 781.28	0.03
$11_{6,6}-10_{5,5}$							126 244.35	−0.10		
$11_{5,6}-10_{6,5}$							126 186.18	−0.33		
$12_{2,11}-11_{1,10}$							109 769.52	0.04	108 263.43	−0.11
$12_{0,12}-11_{1,11}$	106 287.86	0.07					103 590.82	0.01		
$12_{3,10}-11_{2,9}$									114 633.60	0.14
$12_{1,11}-11_{2,10}$	113 044.86	0.08	108 678.13	0.06	109 031.11	0.03				
$12_{2,10}-11_{3,9}$			115 147.92	0.04			115 949.52	0.07		
$13_{1,13}-12_{0,12}$	114 862.70	0.01	110 459.10	0.03			111 965.08	0.11	110 118.97	0.00
$13_{1,12}-12_{2,11}$			116 925.02	0.00	117 333.53	−0.14	118 143.40	−0.05	116 488.24	−0.11
$14_{1,14}-13_{0,13}$			118 705.95	−0.14					118 343.75	0.04
$15_{2,13}-15_{1,14}$							83 351.71	−0.02		
$16_{3,13}-16_{2,14}$							83 311.94	−0.02		
$21_{8,13}-21_{7,14}$							82 981.79	0.03		
$16_{1,15}-16_{0,16}$	104 704.70	−0.09								
$17_{2,15}-17_{1,16}$	104 670.84	0.13								
$18_{3,15}-18_{2,16}$	104 631.70	−0.05								
$19_{4,15}-19_{3,16}$	104 585.96	0.02								
$20_{5,15}-20_{4,16}$	104 533.30	−0.02								
$21_{6,15}-21_{5,16}$	104 472.77	0.05								
$22_{7,15}-22_{6,16}$	104 403.85	−0.03								
$17_{1,16}-17_{0,17}$	111 460.76	0.01	106 619.77	−0.05	103 237.43	0.03			105 087.21	−0.04
$18_{2,16}-18_{1,17}$	111 426.98	0.04	106 548.83	−0.03	103 211.60	0.02	101 885.74	−0.02	105 072.00	0.06
$19_{3,16}-19_{2,17}$	111 388.08	−0.11	106 465.94	−0.06			101 847.18	0.13	105 054.83	−0.03
$20_{4,16}-20_{3,17}$	111 343.00	0.04	106 369.56	0.03			101 803.13	0.01	105 035.19	−0.01
$21_{5,16}-22_{4,17}$	111 291.64	0.00							105 013.00	−0.03
$22_{6,16}-22_{5,17}$	111 233.22	−0.09								
$23_{7,16}-23_{6,17}$	111 166.80	0.05								
$24_{8,16}-24_{7,17}$	111 092.02	0.06								
$25_{9,16}-25_{8,17}$	111 008.07	0.00								
$26_{10,16}-26_{9,17}$	110 914.12	−0.09								
$27_{11,16}-27_{10,17}$	110 809.18	−0.06							104 811.09	0.04
$28_{12,16}-28_{11,17}$	110 692.40	0.05							104 763.49	−0.07
$29_{13,16}-29_{12,17}$									104 710.78	0.09
$18_{1,17}-18_{0,18}$			113 084.60	0.06			108 096.54	0.08	111 455.88	0.06
$19_{2,17}-19_{1,18}$			113 014.11	0.04	109 469.03	−0.16	108 063.22	−0.01	111 440.46	0.02
$20_{3,17}-20_{2,18}$			112 932.45	0.01	109 439.04	0.01	108 024.93	−0.02	111 423.05	−0.05
$21_{4,17}-21_{3,18}$					109 405.06	0.04	107 981.23	0.01	111 403.32	−0.02
$22_{5,17}-22_{4,18}$					109 366.60	0.01	107 931.67	0.00	111 381.20	−0.02
$23_{6,17}-23_{5,18}$					109 323.18	−0.01			111 356.47	−0.04
$24_{7,17}-24_{6,18}$							107 812.67	−0.04	111 328.84	0.00
$26_{9,17}-26_{8,18}$			112 134.29	0.01	109 158.41	0.29				
$27_{10,17}-27_{9,18}$			111 935.84	0.00	109 090.99	−0.10				
$28_{11,17}-28_{10,18}$			111 713.99	−0.01						
$30_{13,17}-30_{12,18}$					108 840.69	0.31				
$31_{14,17}-31_{13,18}$					108 739.81	−0.30				
$19_{1,18}-19_{0,19}$					115 752.29	0.00			117 824.52	0.06
$20_{2,18}-20_{1,19}$					115 725.91	0.04	114 240.61	−0.14	117 808.65	0.08
$21_{3,18}-21_{2,19}$					115 695.99	0.07	114 202.16	−0.01	117 790.97	−0.02

Table I (Continued)

transition	$^{13}CH_2{}^{13}CH_2OOO$		$CH_2CH_2{}^{18}O{}^{18}O{}^{18}O$		*trans*-CHDCHDOOO		*cis,endo*-CHDCHDOOO		*cis,exo*-CHDCHDOOO	
$J'_{K_{-1},K_{+1}} - J''_{K_{-1},K_{+1}}$	ν_{obsd}[a]	$\Delta\nu$[b]	ν_{obsd}[a]	$\Delta\nu$[b]	ν_{obsd}[a]	$\Delta\nu$[b]	ν_{obsd}[a]	$\Delta\nu$[b]	ν_{obsd}[a]	$\Delta\nu$[b]
$22_{4,18}-22_{3,19}$					115 662.32	−0.03	114 158.73	0.03	117 771.05	0.03
$23_{5,18}-23_{4,19}$					115 624.30	−0.01	114 109.91	0.01	117 748.95	−0.01
$24_{6,18}-24_{5,19}$					115 581.82	−0.13	114 055.10	−0.02	117 724.31	0.03
$25_{7,18}-25_{6,19}$					115 534.18	−0.07	113 993.79	−0.04	117 697.12	−0.03
$29_{10,19}-29_{9,20}$							119 952.52	0.01		
$29_{9,20}-29_{8,21}$							126 215.56	0.02		

[a] The estimated uncertainty in the frequency measurements is 0.2 MHz. [b] $\Delta\nu$ is the observed minus calculated frequency from the least-squares fit. [c] Not included in fit.

Table II. Rotational Constants (MHz) and Centrifugal Distortion Parameters (MHz) of Carbon-13, Oxygen-18, and Deuterium Isotopomers of Ethylene Primary Ozonide[a]

	$^{13}CH_2{}^{13}CH_2OOO$	$CH_2CH_2{}^{18}O{}^{18}O{}^{18}O$	*trans*-CHDCHDOOO	*cis,endo*-CHDCHDOOO	*cis,exo*-CHDCHDOOO
A	7947.778 (9)	7786.184 (3)	7515.04 (1)	7544.00 (2)	7464.542 (9)
B	7407.19 (2)	6878.494 (3)	7063.613 (8)	7031.64 (2)	7139.83 (1)
C	4288.07 (1)	4124.336 (4)	4152.02 (1)	4187.768 (6)	4113.060 (6)
Δ_J	0.00165 (5)	0.00164 (2)	0.00145 (6)	0.00167 (8)	0.00145 (4)
Δ_{JK}	0.0011 (1)	0.00104 (6)	0.0011 (1)	0.0013 (3)	0.0009 (1)
δ_J	0.00050 (1)	0.00045 (1)	0.00038 (2)	0.00047 (4)	0.00042 (2)
δ_K	0.00178 (2)	0.00170 (1)	0.00151 (2)	0.00177 (2)	0.00132 (1)

[a] Uncertainties in parentheses are one standard deviation of the least-squares fit.

Table III. Rotational Transitions (MHz), Rotational Constants (MHz), and Centrifugal Distortion Constants (MHz) of Ethylene-d_4 Primary Ozonide

transition $J'_{K_{-1},K_{+1}} - J''_{K_{-1},K_{+1}}$	ν_{obsd}[a]	$\Delta\nu$[b]
$8_{8,1}-7_{7,0}$	109 528.81	0.02
$10_{5,5}-9_{6,4}$	110 174.29	0.79
$10_{6,5}-9_{5,4}$	110 224.10	−1.35
$12_{1,11}-11_{2,10}$	103 058.39	0.33
$13_{1,13}-12_{0,12}$	105 224.61	−0.42
$19_{1,18}-19_{0,19}$	105 580.59	−0.75
$20_{2,18}-20_{1,19}$	105 567.35	−0.42
$21_{3,18}-21_{2,19}$	105 552.51	−0.13
$22_{4,18}-22_{3,19}$	105 536.12	−0.07
$23_{5,18}-23_{4,19}$	105 517.40	0.38
$24_{6,18}-24_{5,19}$	105 496.85	0.55
$21_{2,19}-21_{1,20}$	111 273.87	−0.58
$22_{3,19}-22_{2,20}$	111 258.69	−0.17
$23_{4,19}-23_{3,20}$	111 241.86	0.19
$24_{5,19}-24_{4,20}$	111 223.08	0.67
$25_{6,19}-25_{5,20}$	111 202.57	0.91
$26_{7,19}-26_{6,20}$	111 179.94	1.12
$27_{8,19}-27_{7,20}$	111 155.09	2.97
$28_{9,19}-28_{8,20}$	111 127.90	−5.26

spectral constants (MHz)

A	6937.26 (13)[c]	Δ_J	0.0012 (9)
B	6652.57 (33)	Δ_{JK}	−0.0009 (7)
C	3937.40 (27)	δ_J	0.00055864[d]
		δ_K	0.0009 (3)

[a] The estimated uncertainty in the frequency measurements is 0.2 MHz. [b] $\Delta\nu$ is the observed minus calculated frequency from the least-squares fit. [c] The uncertainties in parentheses are one standard deviation of the least-squares fit. They are large compared to the isotopic species listed in Table II because of the lack of sufficient R-branch lines in the fit. [d] Fixed at the value determined for the normal isotope.

many of the nonplanar ring conformations. For example, Hiberty compared an oxygen envelope form to the carbon–carbon half-chair, determining the latter to be higher in energy by 1 to 3 kcal/mol depending upon the choice of basis set.[10c]

Cremer investigated the potential surfaces of primary ozonides and secondary ozonides using single determinant restricted Hartree–Fock theory.[10e] This method was previously shown to yield reasonable conformational energies for H_2O_2 and H_2O_3 and also to be good models for the study of POs and SOs. Large augmented basis sets including polarization functions and complete geometry optimization of the conformational parameters were required to determine the surfaces. Contrary to previous quantum

Table IV. Atomic Coordinates (Å) of Ethylene Primary Ozonide

atom	coordinate	p-r_s[a]	r_0[b]
carbon	*a*	±0.7729	±0.7784
	b	−0.9750	−0.9789
	c	0.0930	0.0889
$oxygen_{1,3}$	*a*	±1.1139	±1.1156
	b	0.3571	0.3670
	c	−0.2476	−0.2459
$oxygen_2$	*a*	0.0000	0.0000
	b	1.1066	1.0937
	c	0.3072	0.3099
$hydrogen_{endo}$	*a*	±1.1648	±1.1667
	b	−1.2312	−1.2398
	c	1.0751	1.0768
$hydrogen_{exo}$	*a*	±1.2057	±1.2076
	b	−1.6059	−1.6066
	c	−0.6905	−0.6927

[a] The carbon *a* and *b* coordinates, the $oxygen_{1,3}$ *a* coordinate, and all hydrogen coordinates were determined by the substitution method. The remaining coordinates were obtained from a least-squares fit to the moment relations (see text). [b] The r_0 coordinates were obtained from a least-squares fit of all the effective second moment data and the useful moment relations.

chemical calculations the oxygen envelope form (C_s symmetry) of ethylene PO was found to be lowest in energy which is consistent with the microwave data. In the case of ethylene SO, the oxygen–oxygen half-chair conformation (C_2 symmetry) was determined to be the most stable form in agreement with microwave results.

Further support for Cremer's ab initio MO calculations comes from a comparison of the theoretical and microwave structural parameters of ethylene PO and SO. There is good agreement between the experimental and ab initio ethylene PO structures listed in Table V. In addition, Cremer has noted the reasonable agreement between the experimental and theoretical geometries of ethylene SO.

Recent SCF and MCSCF calculations by Ruoff, Saebo, and Almlof have employed a Gaussian double-zeta (ζ) basis set to investigate the energies of seven ethylene PO conformers including the planar and oxygen envelope (C_s symmetry) configurations.[10h,i] The SCF results show very small energy differences for the seven ring forms with the oxygen envelope corresponding to the energy minimum. However, the MCSCF calculations put the oxygen envelope, carbon–carbon half-chair and planar conformers considerably higher in energy than the other four puckered forms. The activation energy for the ozone plus ethylene addition is

Table V. Interatomic Distances (Å) and Angles (deg) of Ethylene Primary Ozonide

parameter	$p\text{-}r_s$[a]	r_0[b]	theoretical[c]
C–C	1.546 (3)	1.557 (3)	1.551
C–O	1.417 (4)	1.427 (3)	1.437
O–O	1.453 (3)	1.443 (3)	1.454
$C\text{–}H_{endo}$	1.088 (2)	1.093 (3)	1.09
$C\text{–}H_{exo}$	1.095 (2)	1.090 (4)	1.09
θ(CCO)	103.9 (1)	103.7 (1)	104.1
θ(COO)	102.1 (2)	101.7 (2)	102.3
θ(OOO)	100.1 (2)	101.3 (2)	101.3
$\theta(CCH_{endo})$	111.1 (2)	110.8 (2)	111.9
$\theta(CCH_{exo})$	113.3 (1)	113.2 (2)	113.4
θ(HCH)	111.6 (3)	111.8 (3)	
Φ[d]	50.85	51.38	

[a] The $p\text{–}r_s$ parameters were calculated from the $p\text{–}r_s$ coordinates in Table III employing a combination of Costain and least-squares fitting uncertainties in the atomic coordinates to obtain the propagated errors given in parentheses. [b] The r_0 parameters were determined from the r_0 coordinates in Table III. The errors in parentheses were propagated from the uncertainties in r_0 coordinates. [c] The theoretical parameters are taken from an ab initio calculation in ref 10e. [d] Φ is the oxygen envelope angle as shown in Figure 1.

calculated to be very high at 23.5 kcal/mol compared to experimental and other theoretical determinations which fall in the range of a few kcal/mol.[9c,22-24]

The MCSCF results are likely not consistent with experimental data and Cremer's ab initio calculations due to the use of an inadequate basis set. Hartree–Fock calculations which use large Gaussian double-ζ basis sets do not give a trans barrier in hydrogen peroxide. The studies show that scaled polarization functions with complete geometry optimization are needed to correctly describe the barrier to internal rotation in hydrogen peroxide.[25] Cremer found that similar conclusions follow from results for the related species, H_2O_3.[26]

Molecular Structure. The CO, OO, and CC bond distances obtained here for ethylene PO fall within the range of values reported for related compounds. As shown in Table VI the CO distance for ethylene PO is virtually the same in ethylene SO (true for both the CO epoxy and peroxy bonds). They are quite consistent with the range of 1.41–1.44 Å usually observed for CO single bonds.

The OO distance for ethylene PO appears to be low when compared to related compounds for which spectroscopic data are available. These species include hydrogen peroxide, ethylene SO, and propylene SO. However, OO distances obtained primarily from X-ray diffraction work are 1.44–1.48 Å with uncertainties of 0.01–0.04 Å.[27] Hence, the OO distance in ethylene PO does not seem to be unusual for an OO single bond.

There are not many compounds like ethylene PO to compare CC bonds. However, the CC distance of 1.546 Å is within the range of typical CC single bonds. It also compares favorably to the CC bond lengths for the saturated five-membered rings, tetrahydrofuran and 1,3-dioxa-2-borolane listed in Table VI.

Ring-Puckering Vibrations. The spectral assignments of two excited vibrational states of ethylene PO were described in the preliminary microwave study.[11] The observed transitions fit well to a centrifugal distortion model and the two states $v = 1$ and $v = 2$ were calculated by relative intensity measurements to be 98 (6) and 171 (18) cm^{-1}, respectively, above the ground state. The differences in the rotational constants $A_v - A_0$, $B_v - B_0$, and $C_v - C_0$ versus v are nearly linear as shown in Figure 2. Transitions from the $v = 3$ state were observed but not assigned due to the lack of enough intense lines for the centrifugal distortion analysis.

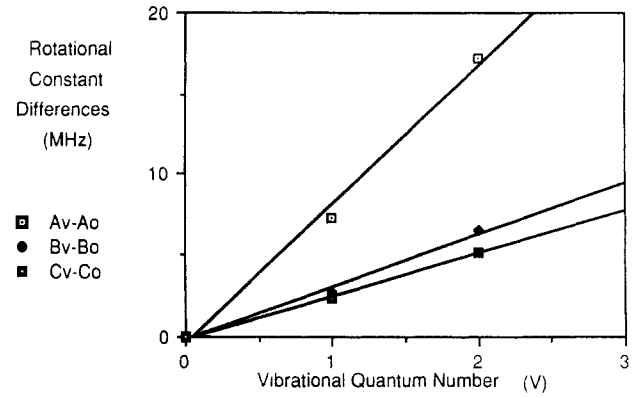

Figure 2. Differences in the rotational constants $A_v - A_0$, $B_v - B_0$, and $C_v - C_0$ in MHz versus vibrational states for successive vibrational excitations of the pseudorotational mode in ethylene PO.

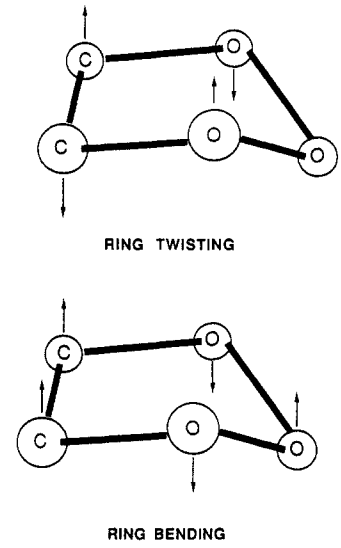

Figure 3. The ring atomic displacements for the pseudorotational (ring twisting) and radial (ring bending) modes of ethylene PO in the oxygen envelope configuration.

These results support the assignment of the vibrational states to a ring-puckering mode.

The two ring-puckering modes in saturated five-membered rings can be described in terms of radial and pseudorotational coordinates.[28] The motion of the radial coordinate corresponds to an oscillation of the amplitude of puckering about the lowest energy ring conformation. It is higher in energy than the pseudorotational mode. The latter vibration is unusual because the motion is one in which the phase of the puckering rotates around the ring. By alternating between bent and twisted ring configurations, the molecule undergoes a ring inversion without ever going through the planar ring form. In the radial mode, a simple bend or twist through the planar configuration inverts the ring. For five-membered rings, barriers to ring inversion are encountered for both the pseudorotational and radial modes.[29]

Strong vibration–rotation interactions are observed in the rotational spectra of pseudorotational states for tetrahydrofuran[30] and 1,3-dioxolane.[31] In these cases, the barriers hindering pseudorotation are small (<100 cm^{-1}) relative to the very high barrier to ring inversion through planarity. Most other five-membered rings[28] including ethylene SO[32] have high barriers to

(22) Cremer, D. *J. Am. Chem. Soc.* **1981**, *103*, 3619.
(23) Wadt, W. R.; Goddard, W. A., III *J. Am. Chem. Soc.* **1975**, *97*, 3004.
(24) Nangia, P. S.; Benson, S. W. *J. Am. Chem. Soc.* **1980**, *102*, 3105.
(25) (a) Davidson, R. B.; Allen, L. C. *J. Chem. Phys.* **1971**, *55*, 519. (b) Dunning, Jr., T. H.; Winter, N. W. *J. Chem. Phys.* **1975**, *63*, 1847. (c) Cremer, D. *J. Chem. Phys.* **1978**, *69*, 4440.
(26) Cremer, D. *J. Chem. Phys.* **1978**, *69*, 4456.
(27) Petersen, B. F. *Acta Crystallogr., Sect. B* **1972**, *28*, 1014.
(28) Laane, J. *Vibrational Spectra and Structure*; Durig, J. R., Ed.; Marcel Dekker: New York, 1972; chapter 2.
(29) Harris, D. O.; Engerholm, G. G.; Tolman, C. A.; Luntz, A. C.; Keller, R. A.; Kim, H.; Gwinn, W. D. *J. Chem. Phys.* **1969**, *50*, 2438.
(30) Engerholm, G. G.; Luntz, A. C.; Gwinn, W. D.; Harris, D. O. *J. Chem. Phys.* **1969**, *50*, 2446.
(31) Baron, P. A.; Harris, D. O. *J. Mol. Spectrosc.* **1974**, *49*, 70.

Table VI. Comparison of CO, OO, and CC Bond Lengths (Å) for Ethylene PO with Related Compounds

compound	*R*(CO)	*R*(OO)	*R*(CC)	method[a]	ref
ethylene PO	1.417	1.453	1.546	MW	this work
ethylene SO	1.416_{epoxy} 1.412_{peroxy}	1.461		MW	19, p 678
propylene SO	1.423_{epoxy} $1.411_{peroxy\ CH_2}$	1.471		MW	*b*
tetrahydrofuran	1.428		1.538	ED	*c*
1,3-dioxa-2-borolane	1.438		1.541	MW	19, p 679
hydrogen peroxide		1.467		IR	*d*
methanol	1.425			MW	19, p 663
dimethyl ether	1.410			MW	19, p 682

[a] MW = microwave, ED = electron diffraction, and IR = infrared. [b] Lattimer, R. P.; Kuczkowski, R. L.; Gillies, C. W. *J. Am. Chem. Soc.* **1974**, *96*, 348. [c] Almenningen, A.; Seip, H. M.; Willadsen, T. *Acta Chem. Scand.* **1969**, *23*, 2748. [d] Giguere, P. A.; Srinivasan, T. K. K. *J. Mol. Spectrosc.* **1977**, *66*, 168.

Table VII. Low-Energy Conformations and Barriers to Ring Inversion of Oxygen-Containing Five-Membered Rings

compound	lowest energy conformation	barrier to pseudorotation, cm^{-1}	barrier to planarity, cm^{-1}	method and reference
tetrahydrofuran	C–C half-chair (C_2 symmetry)	57	1220	microwave, 30
$\overbrace{CH_2CH_2CH_2CH_2O}$	C–C half-chair (C_2 symmetry)	105	924	ab initio MO, 33
1,3-dioxolane	carbon envelope (C_s symmetry)	45		microwave, 31
$\overbrace{CH_2CH_2OCH_2O}$	C–C half-chair (C_2 symmetry)	363	412	ab initio MO, 33
ethylene SO	O–O half-chair (C_2 symmetry)	>500–600		microwave 31
$\overbrace{CH_2OCH_2OO}$	O–O half-chair (C_2 symmetry)	1050		ab initio MO, 10e
ethylene PO	oxygen envelope (C_s symmetry)	>300–400		microwave this work
$\overbrace{CH_2CH_2OOO}$	oxygen envelope (C_s symmetry)	1225	2700	ab initio MO, 10e

pseudorotation (> several hundred wavenumbers). In these cases, the ring-puckering states do not exhibit significant vibration–rotation interactions. Furthermore, the motions of the pseudorotational and radial modes for the high barrier cases are described in terms of Cartesian out-of-plane bending and twisting coordinates about an equilibrium bent or twisted conformation.[29] The ring atom displacements are shown in Figure 3 for the bent oxygen envelope form of ethylene PO.

The microwave data allow an assignment of the observed vibrational states to the lower energy ring-puckering mode. Since the rotational spectra of the $v = 0$, 1, and 2 states do not exhibit perturbations due to vibration–rotation interactions, the pseudorotational barrier and barrier to planarity must be high (greater than 300 to 400 cm^{-1}). The ground-state conformation of ethylene PO is the bent oxygen envelope form (Figure 1). Hence, the lowest energy ring-puckering mode in ethylene PO corresponds to the ring-twisting vibration illustrated in Figure 3. Since no other intense vibrational states could be assigned for ethylene PO, the higher energy ring-bending mode is estimated to be above 200 cm^{-1}.

Table VII compares the lowest energy conformations and barriers to ring inversion through pseudorotation and planarity for a series of five-membered rings containing oxygen. Both tetrahydrofuran and 1,3-dioxolane have low barriers to pseudorotation with the twisted form (C_2 symmetry) about 35 cm^{-1} below a bent form in tetrahydrofuran[30] and the bent form about 10 cm^{-1} below a twisted conformer in 1,3-dioxolane.[31] Since the barrier to planarity was estimated to be 1220 cm^{-1}, tetrahydrofuran is able to invert the ring through the very low energy pseudorotational barrier of 57 cm^{-1}. Ethylene SO and PO are both high barrier cases and the lowest energy conformations are the C–C half-chair (C_2 symmetry)[32] and the oxygen envelope (C_s symmetry)[11] forms, respectively.

The ab initio molecular orbital calculations by Cremer determined the pseudorotational potential surfaces of all four oxygen-containing species listed in Table VII as well as that of cyclopentanone.[33] There is reasonable agreement between the microwave and ab initio results for tetrahydrofuran. In the case of 1,3-dioxolane, the MO calculations find the planar barrier to be similar to the pseudorotational barrier through a carbon envelope configuration. These results differ from the experimental studies on 1,3-dioxolane which show a very low barrier to pseudorotation through the C–C half-chair conformer. The microwave and ab initio MO calculations both find the barriers to pseudorotation to be high for ethylene SO and PO. Ring inversion through the planar configuration was found to be approximately a factor of 2 less favorable with calculated barriers of 2100 and 2700 cm^{-1}, respectively, for ethylene SO and PO.[10e]

While microwave data are not sensitive to the barrier heights for high barrier cases like ethylene SO and PO, it is possible to accurately obtain these barriers with far-infrared and Raman techniques. Using far-infrared data, Ikeda and Lord found that the cyclopentanone ring inverts between two equivalent twisted conformations (C_2 symmetry) through a planar barrier of 750 cm^{-1}.[34] The pseudorotational barrier is considerably higher at 1290 cm^{-1}. Ab initio MO calculations for cyclopentanone give values of 907 and 1290 cm^{-1}, respectively, for the pseudorotational and planar barriers.[33] Durig et al. used far-infrared and Raman data to show that ring inversion between the most stable twisted conformations (C_2 symmetry) of germacyclopentane occurs through a slightly bent configuration with a barrier of 1454 cm^{-1}.[35] This pseudorotational barrier is only 20 cm^{-1} less than the barrier to ring inversion through the planar conformation. Far-infrared and Raman data are needed to determine the potential surfaces of ethylene SO and PO for comparison with the ab initio MO results.[10e]

Electric Dipole Components. Few molecules containing the O–O–O linkage have been studied by microwave spectroscopy. For this reason, the O_2–$O_{1,3}$ electric bond moment is not known.

(32) Gillies, C. W.; Kuczkowski, R. L. *J. Am. Chem. Soc.* **1972**, *94*, 6337.

(33) Cremer, D.; Pople, J. A. *J. Am. Chem. Soc.* **1975**, *97*, 1358.
(34) Ikeda, T.; Lord, R. C. *J. Chem. Phys.* **1972**, *56*, 4450.
(35) Durig, J. R.; Li, Y. S.; Carreira, L. A. *J. Chem. Phys.* **1973**, *58*, 3293.

An exception is ozone where the molecular structure[19] and electric dipole moment[36] give a value of 0.509 D for the O_2–$O_{1,3}$ moment. If the H–C bond moment is fixed in ethylene PO, the C–O and O_2–$O_{1,3}$ moments may be calculated from the observed μ_b and μ_c electric dipole components and the molecular structure listed in Table VI.

H–C bond moments have been calculated from microwave data for series of oxirane and ethylene SO derivatives. The calculated H–C moments vary from 0.33 D in ethylene oxide[37] to 0.44 D in ethylene SO.[38] If 0.40 D is assumed for the H–C moment in ethylene PO, the C–O and O_2–$O_{1,3}$ bond moments are calculated to be 1.30 and −0.33 D, respectively. This calculation assumed μ_b to be positive and μ_c to be negative. All other dipole component sign combinations give unreasonable values for the magnitude and/or the direction of the C–O moment. Varying the H–C bond moment from 0.30 to 0.50 D gives a range of 0.34 to 0.33 D in the O_2–$O_{1,3}$ moment and a range of 1.38 to 1.21 D in the C–O moment.

The O_2–$O_{1,3}$ moment in ethylene PO (0.33 D) is similar in magnitude but opposite in sign to the O_2–$O_{1,3}$ moment in ozone (0.51 D). Interestingly, the central oxygen is more negative than the oxygens bonded to the carbons of ethylene PO in the calculation described above. In the case of ozone, Zeeman effect measurements suggest that the central oxygen is more positive.[36a] The C–O bond moment in ethylene PO falls between the values of 0.92 D determined for ethylene oxide and 1.72 D calculated for ethylene SO. The magnitudes of the C–O and O_2–$O_{1,3}$ bond moments should be significantly affected by the orientations of the lone electron pairs on the oxygen atoms in these ring compounds.

Mechanism of Ethylene Ozonolysis. In this section, a mechanism of the reaction of ozone with ethylene is proposed which rationalizes the results for the conditions present in the low-temperature microwave cell. The data suggest that the reaction occurs primarily in the condensed phase on the surface of the microwave cell where efficient vibrational quenching of products takes place. As shown in reaction 4, ozone adds to ethylene to produce vibrationally hot ethylene PO at temperatures of −175 to −170 °C. The formation of ethylene PO is exothermic by roughly −50 kcal/mol[24] and it is known from condensed-phase IR studies that the initial reaction proceeds at temperatures as low as 80 K.[9c,h]

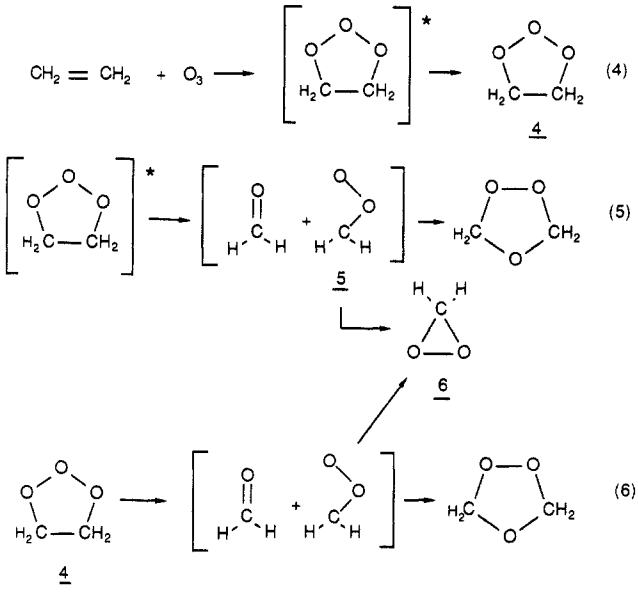

Since thermalized gas-phase rotational spectra of ethylene PO are observed between −110 and −90 °C, the formation and subsequent vibrational quenching of **1** must occur at lower temperatures. In addition the microwave cell pressure of 50 μm is far too low for significant collisional stabilization of the hot ethylene PO in the gas phase.[5] Hence, the quenching of hot ethylene PO occurs in the condensed phase as shown in reaction 4. These processes take place below −130 °C because formaldehyde, ethylene SO, and dioxirane exhibit microwave spectra in the range of −130 to −110 °C.

The microwave work shows that ethylene PO is thermally stable up to about −90 °C. This result agrees with IR studies which find ethylene PO decomposes in the range of −100 to −80 °C.[9a] The formation of formaldehyde, ethylene SO, and dioxirane at temperatures below the decomposition of **4** can be explained by reaction 5. Cleavage of hot ethylene PO will give formaldehyde and dioxymethylene **5**. Addition of formaldehyde to **5** produces ethylene SO while ring closure of **5** yields dioxirane **6**. Condensed-phase IR studies with ethylene ozonolysis[9a] and NMR solution studies of small alkene ozonolyses[8c] show that a portion of the hot primary ozonide is not stabilized and cleaves to produce aldehydes and secondary ozonides below the thermal decomposition temperatures of the primary ozonides. Both ethylene SO and dioxirane are produced vibrationally hot due to the exothermicities of their formation in reaction 5. Quenching of these products is also expected to occur in the condensed phase at microwave cell pressures of 50 μm.[5]

As shown in reaction 6, thermal decomposition of ethylene PO gives ethylene SO and dioxirane. Condensed-phase IR studies of ethylene ozonlysis[9a,c,h] and solution NMR work on small alkene ozonolyses[8c] clearly show that secondary ozonides are major products from thermal decompositions of primary ozonides. It is difficult by microwave techniques to determine the importance of reaction 6 in the formation of ethylene SO. However, the microwave results do suggest that dioxirane is produced from the thermal decomposition of ethylene PO, possibly by ring closure of **5** as shown in reaction 6. At −100 °C the rotational spectrum of ethylene PO can be observed for a number of hours while continuously pumping on the microwave cell. During this period of time, the microwave spectrum of dioxirane almost completely disappears presumably owing to distillation of the dioxirane produced by reaction 5 from the cell. At temperatures above −90 °C, the dioxirane spectrum reappears while the ethylene PO spectrum disappears.

If dioxirane is produced from ring closure of **5**, it is likely that the reaction takes place in the condensed phase. Dioxirane is estimated to be 46 kcal/mol more stable than dioxymethylene **2**.[5] The exothermicity of the reaction is so large that vibrational quenching is necessary to stabilize dioxirane, and the microwave cell pressures are too low to provide collisional stabilization in the gas phase.[5] Isotopic labeling experiments are currently underway to determine whether dioxirane acts as an intermediate in the formation of ethylene SO.

Reaction 4, which is the first step in the ozonolysis mechanism is postulated to be a concerted 1,3-dipolar cycloaddition of ozone to the carbon–carbon double bond. There is strong evidence that ozone adds stereospecifically to a number of dialkyl-substituted alkenes. The most conclusive evidence comes from a combination of NMR and chemical studies of the formation and reduction of POs.[1,3] The present work demonstrates directly by microwave techniques that ozone does indeed add to ethylene in a stereospecific manner to form ethylene PO.

The microwave evidence comes from the reaction of ozone with isomerically pure *trans*- and *cis*-1,2-dideuterioethylene shown in reactions 7 and 8. Ozone adds to *trans*-CHD=CHD stereospecifically to give exclusively *trans*-$\overline{\text{CHDCHDOOO}}$. Similarly, *cis*-CHD=CHD reacts with ozone to give exclusively *cis,endo*- and *cis,exo*-$\overline{\text{CHDCHDOOO}}$. Strong lines from the trans and two cis $\overline{\text{CHDCHDOOO}}$ isotopic species were used to set lower limits of 1–2% for the amount of *trans*-$\overline{\text{CHDCHDOOO}}$ in the *cis*-

(36) (a) Pochan, J. M.; Stone, R. G.; Flygare, W. H. *J. Chem. Phys.* **1969**, *51*, 4278. (b) Mack, K. M.; Muenter, J. S. *J. Chem. Phys.* **1977**, *66*, 5278.
(37) Agopovich, J. W.; Alexander, J.; Gillies, C. W.; Raw, T. T. *J. Am. Chem. Soc.* **1984**, *106*, 2250.
(38) LaBarge, M. S.; Hillig, K. W., II; Kuczkowski, R. L. *J. Phys. Chem.* **1986**, *90*, 3092.

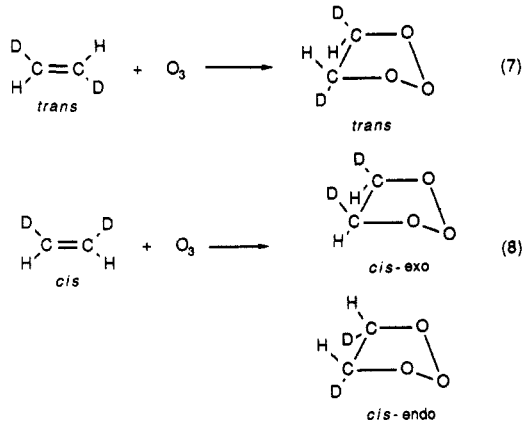

CHD=CHD reaction and of *cis*-CHDCHDOOO in the *trans*-CHD=CHD reaction. These limits are within the estimated isomeric purity of the *cis*- and *trans*-CHD=CHD samples.

Appendix

Many molecules which are nearly prolate rotors are found to exhibit bands under low resolution conditions.[39] These bands follow symmetric top frequency rules and consist of overlapping transitions arising from either μ_a dipole-allowed R-branch lines or less commonly from μ_b- and/or μ_c-type Q-branch lines. The μ_b- and/or μ_c-type bands follow the symmetric top expression in the equation:

$$\nu_{band} = (2A - B - C)(K_{-1} + \tfrac{1}{2}) \qquad \text{(III)}$$

where ν_{band} is the band frequency, A, B, and C are the rotational constants, and K_{-1} is the quantum number for quantization of rotational angular momentum about the symmetry axis.[40] Rigid rotor theory has been applied to μ_b- and μ_c-type Q-branch lines to understand the composition and characteristics of the bands given by eq III.[41]

Analogous Q-branch transitions are possible for nearly oblate rotors with nonzero μ_a- and/or μ_b-electric dipole components. As shown by the four level system in Figure 4, the μ_a- and μ_b-type lines form four different Q-branch series. In all four series, $\Delta J = 0$ and $\Delta K_{+1} = -1$ so that the μ_a-type transitions involve the $J(J - K_{+1} + 2, K_{+1}) \leftarrow J(J - K_{+1}, K_{+1} + 1)$, and $J(J - K_{+1} + 1, K_{+1}) \leftarrow J(J - K_{+1} + 1, K_{+1} + 1)$ levels. Analogous μ_b-type transitions go from the $J(J - K_{+1}, K_{+1} + 1)$ level to the $J(J - K_{+1} + 1, K_{+1})$ level and the $J(J - K_{+1} + 1, K_{+1} + 1)$ level to the $J(J - K_{+1} + 2, K_{+1})$ level. The rotational energy levels of a nearly oblate rigid rotor are given by the expression

$$E_{J,K_{-1},K_{+1}} \simeq (A + B)(J + 1)J/2 + [C - (A + B)/2]K_{+1}$$

in the zeroth-order approximation.[42] Application of the selection rules $\Delta J = 0$ and $\Delta K_{+1} = -1$ to all four series leads to the frequency expression given in the Results as eq I. Hence under low-resolution conditions, nearly oblate rotors with strong μ_a- and/or μ_b-type transitions may give bands that follow the frequency rule in eq I.[43] In cases such as ethylene PO where individual lines are seen up to the series origin, the expression is useful for determining the K_{+1} quantum numbers which are involved in the μ_a- and/or μ_b-type transitions. Figure 5 illustrates a nice example of the $K_{+1} = 15 \leftarrow 16$, μ_b-type Q-branch series for ethylene SO. The first six members of the ground state beginning with the $16_{1,15} \leftarrow 16_{0,16}$ transition along with several vibrational satellites of the low-lying pseudorotational mode are shown in Figure 5.

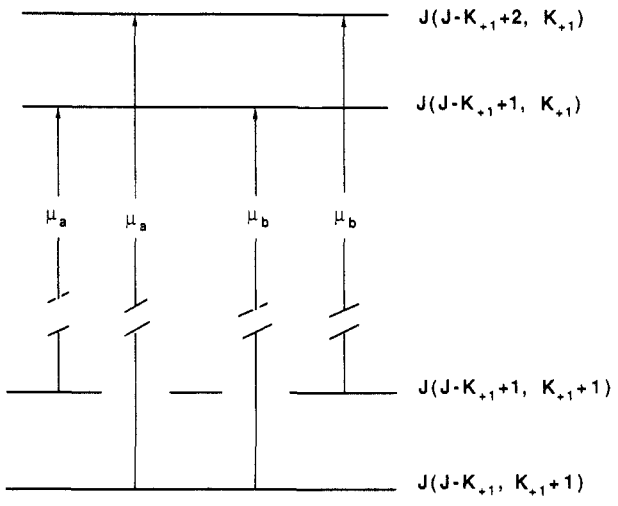

Figure 4. The rotational levels for μ_a- and/or μ_b-dipole Q-branch transitions of nearly oblate tops.

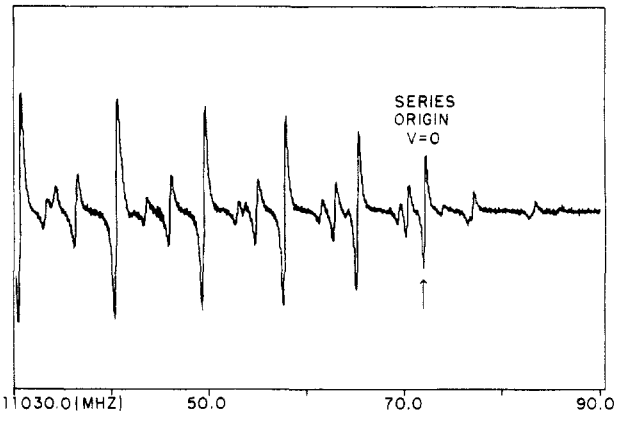

Figure 5. The $K_{+1} = 15 \leftarrow 16$ μ_b-type Q-branch series for ethylene secondary ozonide. The series origin for the ground state and several excited vibrational states of the pseudorotational mode begin with the degenerate pair of $16_{2,15} \leftarrow 16_{1,16}$ and $16_{1,15} \leftarrow 16_{0,16}$ transitions. $(A + B - 2C)$ is equal to 7168 MHz (ref 32).

Registry No. 4, 6669-36-9; **5**, 56077-93-1; **6**, 157-26-6; CH_2=CH_2, 74-85-1; H_2C=O, 50-00-0; 1,2,4-trioxolane, 289-14-5; *trans*-D—CH=CH—D, 1517-53-9; *cis*-D—CH=CH—D, 2813-62-9; *trans*-4,5-dideuterio-1,2,3-trioxolane, 117068-65-2; *cis*-4,5-dideuterio-1,2,3-trioxolane, 117068-66-3; 1,2,3-trioxolane-$^{13}C_2$, 117068-67-4; 1,2,3-trioxolane-$^{18}O_3$, 117068-68-5.

(39) Gillies, C. W. *Appl. Spectrosc. Rev.* **1982**, *18*, 1–58.
(40) Steinmetz, W. E. *J. Am. Chem. Soc.* **1974**, *96*, 685.
(41) Dennison, F. T.; Gillies, C. W.; Borchert, S. J. *J. Chem. Phys.* **1981**, *75*, 3238.
(42) Townes, C. H.; Schawlow, A. L. *Microwave Spectroscopy*; McGraw-Hill: New York, 1955; p 86.
(43) In eq I, K_{+1} is equal to $J - 1$ of the lowest J Q-branch transition in each series.